J. Plasma Phys. (2024), *vol*. 90, 905900404
Published by Cambridge University Press
doi:10.1017/S0022377824000783

Spatial distribution of self-seeded air lasers induced by the femtosecond laser filament plasma

Tao Zeng[1],†, **Nan Li**[1] **and Yuliang Yi**[1]

[1]School of Physical Science and Technology, Chongqing key Laboratory of Micro & Nano Structure Optoelectronics, Southwest University, Chongqing 400715, PR China

(Received 31 January 2024; revised 31 May 2024; accepted 3 June 2024)

The femtosecond laser filament-induced air laser plays a significant role for the remote sensing of air pollutants. The spatial distributions of air laser intensity were investigated experimentally in previous studies. However, the mechanism of the air laser propagation properties inside the filament plasma has not been quite clear yet. Moreover, few studies have been dedicated to the reproduction of the air laser profile from nitrogen molecules propagating in the filament plasma based on the numerical simulation method. In this study, the lasing action of the air laser from the transition of the first negative (0,0) band of nitrogen ions at 391 nm was simulated during the femtosecond laser filamentation. The beam profile of the air laser changes from a Gaussian or super-Gaussian shape to an outer ring structure by increasing the filament length or nitrogen ion density, which is in accord with the previous experimental result. A multiple-diffraction effect has been proposed to clarify the mechanism of the outer rings beam pattern formation, which is induced by the dynamical interaction between the lasing effect and diffraction effect of the air laser propagating inside the filament plasma. In addition, the amplified air laser power as a function of both the filament length and nitrogen ion density was investigated. Our study would pave the way to improve the energy conversion efficiency and directivity of remote air lasers, which would be significant for remote sensing applications.

Keywords: femtosecond laser filament, air laser, nitrogen iron density, spatial distribution

1. Introduction

Remote sensing of atmosphere pollutants relies on optical techniques for detecting molecules and atoms based on lasers in order to identify and quantify different species. The light emission collection in the backward direction of the pumped laser is restricted by the non-directional characteristic of the spontaneous emission from molecules of interest. Amplified spontaneous emission based on femtosecond laser filamentation has provided the opportunity to solve this problem and appears as an attractive technique to realize the remote sensing of air pollutants (Luo, Liu & Chin 2003; Dogariu *et al.* 2011; Yuan *et al.* 2013, 2014; Zhang *et al.* 2021; Xue *et al.* 2022). The laser intensity inside a light filament core could remain at more than 10^{13} W cm^{-2} over a very long distance

† Email address for correspondence: taozeng@swu.edu.cn

(Liu 2014). Various species in the atmosphere will be ionized, resulting in the emission of the fingerprint fluorescence. Propagating through the filament, the fluorescence signal could be enhanced, which is referred to as an air laser (Kartashov *et al.* 2012; Ni *et al.* 2013; Zhou *et al.* 2020).

The generation of well-collimated air lasers at 845 nm in the backward and forward directions was investigated with an ultraviolet focused pump beam. By the interaction of the pump beam with molecular oxygen, the doughnut-shaped mode of the air laser was observed with a divergence angle of 40 mrad (Dogariu *et al.* 2011). A super-Gaussian shape of a backward ultraviolet air laser at 337 nm and 357 nm with a divergence angle of 1.6 mrad was produced. The air lasing action results from nitrogen molecules pumped with a high-power midinfrared laser pulse (Kartashov *et al.* 2012). A forward harmonic-seeded air laser from nitrogen molecules driven by intense midinfrared femtosecond laser pulses was reported. The lasing effect refers to the amplification of the harmonic radiation with the presence of population inversion induced by $B^2\sum_u^+ \rightarrow X^2\sum_g^+$ transition between the ground and excited cation states (Yao *et al.* 2011). In addition, the influence of gas pressure on the air laser beam intensity and profile was investigated. It indicates that the forward self-seeded air laser from nitrogen molecules changes from a Gaussian shape to an outer ring pattern with the increase of gas pressure (Liu *et al.* 2013). Moreover, our previous study revealed that a multiple ring pattern of the air laser was generated induced by the nitrogen ions inside a femtosecond laser filament (Zeng *et al.* 2014). However, the mechanism of the propagation properties and spatial distribution of the air laser during the femtosecond laser filamentation has not been quite clear up to now.

In this work, the spatial distribution of the air laser propagating through the femtosecond laser filament plasma has been investigated based on numerical simulation. The result indicates that the air laser beam pattern after the filament changes from a Gaussian or super-Gaussian shape to a multiple outer rings structure by increasing the filament length or nitrogen ion density. Moreover, the number of the outer rings increases versus the filament length or nitrogen ion density. The mechanism of the air laser intensity spatial distribution has been revealed. In addition, the amplified air laser beam power as a function of the filament length and nitrogen ion density has been investigated.

2. Theoretical method

As the nitrogen molecules were ionized to N_2^+ due to multiphoton or tunnel ionization effects during the femtosecond laser filamentation process, the ground state $X^2\sum_g^+$ of the ion was pumped to the excited state $B^2\sum_u^+$. The fluorescence of N_2^+ with a wavelength of 391 nm was stimulated during the vibrational transition of the N_2^+ first negative (0,0) band ($B^2\sum_u^+ \rightarrow X^2\sum_g^+$) (Doering & Yang 1996). The photon density $N_{e,\,391\ \mathrm{nm}}$ of the stimulated fluorescence signal could be derived from the following (Kartashov & Shneider 2017):

$$N_{e,\,391\ \mathrm{nm}} = W_{21}\tau N_{e,\,N_2^+}, \tag{2.1}$$

where $N_{e,\,N_2^+}$ represents the nitrogen ion density; W_{21} and τ denote the probability of the fluorescence emission and the population inversion lifetime, respectively. The fluorescence could be produced only in the region where the nitrogen ion density is larger than a threshold value of 10^{15} cm^{-3}.

In this work, the spatial distribution of the nitrogen ion density in the filament plasma obeys the following equation:

$$N_{e,\,N_2^+}(r, l) = N_{e,\max}\exp\left[-\left(\frac{r^2}{r_0^2}+\frac{l^2}{l_0^2}\right)\right]. \tag{2.2}$$

https://doi.org/10.1017/S0022377824000783 Published online by Cambridge University Press

Here the nitrogen ion density distribution satisfies the cylindrical symmetry. Here r and l refer to the variables of the axis along the radial direction and the longitudinal direction, respectively. Here r_0 is the radius of the filament plasma and is set to be 50 μm in our simulation, which is a common value in the previous studies (Chin et al. 2005; Berge *et al.* 2007; Couairon & Mysyrowicz 2007; Kasparian & Wolf 2008; Kandidov, Shlenov & Kosareva 2009). Here l_0 is the half-length of the filament plasma. Here $N_{e,\max}$ denotes the peak nitrogen ion density. Both l_0 and $N_{e,\max}$ depend on the initial femtosecond laser beam parameters and focusing conditions.

A stationary, homogeneous and isotropic plasma model was selected without considering the temporal variation. The lifetime of the filament plasma is at the nanosecond time scale (Mehr & Biondi 1969; Johnson & Fowler 1970; Brian & Mitchell 1990; Bahati *et al*. 2001; Chauveau *et al.* 2002; Jain, Gupta & Suk 2019), which is much slower than the air laser pulse duration at 391 nm in the picosecond range (Xu *et al.* 2009; Yao *et al.* 2018; Wang *et al.* 2023). Therefore, this simplification of the plasma model is reasonable.

The propagation of the fluorescence from nitrogen molecules at 391 nm in the filament plasma could be based on the following wave equation (Chiron *et al.* 1999):

$$2\mathrm{i}k_0\frac{\partial A}{\partial z}+\left(\frac{\partial^2}{\partial x^2}+\frac{\partial^2}{\partial y^2}\right)A+2\frac{k_0^2}{n_0}n_{\mathrm{nl}}A-\mathrm{i}k_0\alpha A=0, \tag{2.3}$$

where A denotes the air laser amplitude envelope, and k_0 is the air laser wavenumber. Here z represents the air laser propagation distance; n_0 is the air refractive index; n_{nl} refers to the nonlinear refractive index corresponding to the defocusing effect of the filament plasma. The simulation of the air laser propagating in the filament plasma was based on the finite difference method. FORTRAN software was used for conducting the simulation procedure.

It is worth mentioning that since we focused exclusively on the spatial distribution of the air laser, the temporal aspect of the emitted light field was not considered during the simulation. The validity of this simplified model for the nonlinear propagation of a laser pulse has been demonstrated in previous studies (Dubietis *et al.* 2004; Liu & Chin 2007). Thus, temporal effects including self-steeping, group-velocity dispersion effects were neglected in our simulation model. Actually, this kind of simplification would significantly influence the temporal dynamics of the air laser. However, to a lesser extent it would influence the spatial evolution of the air laser in principle, which is clarified as follows. Typically, the air laser radius inside the filament is approximately 50 μm. The corresponding longitudinal scale of spatial transformation $2\pi a^2/\lambda$ is approximately 2 cm. The second-order group velocity dispersion coefficient k'' for air is 0.2 fs^2 cm^{-1} (Akozbek *et al.* 2001). For an air laser pulse with pulse duration at the picosecond time scale (Xu *et al.* 2009; Yao *et al.* 2018; Wang *et al.* 2023), the characteristic dispersion length scale τ^2/k'' of the temporal changes is much longer than the spatial transformation scale. Therefore, the spatial effects develop much faster than the temporal effects and dominate the air laser intensity distribution (Akozbek *et al.* 2001).

The amplitude of the spontaneous fluorescence emission at 391.4 nm at the l position of the filament plasma was denoted by $A_0(l)$. The relative value of $A_0(l)$ was achieved by the square root of the intensity of the fluorescence emission. The fluorescence intensity was proportional to the photon density, which could be derived based on (2.1). The fluorescence signal with amplitude of $A_0(l)$ at $\mathrm{z}=l$ position in the filament plasma would propagate in the filament with a gain effect due to the population inversion of the nitrogen ions, which leads to the air laser with amplitude $A_1(l,z)$ at a propagation distance z position

https://doi.org/10.1017/S0022377824000783 Published online by Cambridge University Press

by conducting the numerical simulation based on (2.3). Then the total air laser amplitude $A_2(z)$ at the z position inside the filament plasma could be derived by the integral of $A_1(l,z)$ along the particular filament length from $l=0$ to $l=z$, as follows:

$$A_2(z) = A_0(z) + \int_{l=0}^{l=z} A_1(l, z). \tag{2.4}$$

Total air laser amplitude $A_2(z)$ at the z position after the filament plasma could be derived as follows:

$$A_2(z) = \int_{l=0}^{l=L_0} A_1(l, z). \tag{2.5}$$

Here, L_0 corresponds to the total filament length.

The nitrogen ions induced by the filamentation could be served as a gain medium for the air laser. Here α corresponds to the gain coefficient of the air laser propagating through the filament plasma, which could be derived based on the following relationship (Sprangle *et al.* 2011):

$$\alpha = \sigma N_{e,\, N_2^+}, \tag{2.6}$$

where σ is the stimulated emission cross-section for the first negative (0,0) band vibrational transition at 391 nm with a constant value of 14.8×10^{-18} cm^2 according to the previous work (Doering & Yang 1996). Finally, the total air laser power at any propagation distance inside or after the filament plasma could be accumulated by the amplified fluorescence emission at any formal filament position with the nitrogen ion density larger than the threshold value.

Population inversion between the vibrational levels of the excited $B^2\sum_u^+$ and the ground $X^2\sum_g^+$ states of the nitrogen molecular ion N_2^+ was achieved, enabling lasing at the 391 nm emission wavelength. The fraction of the inverted $N_2^+ B^2\sum_u^+$ ions was calculated in the previous study, which corresponds to a value of approximately 9 % (Doering & Yang 1996). The fraction of the inverted molecules would influence the $N_2^+ B^2\sum_u^+$ state cross-section. Therefore, both the photon density $N_{e,\,391\ \mathrm{nm}}$ of the stimulated fluorescence signal in (2.1) and the gain coefficient of the air laser in the filament plasma in (2.6) would be influenced by the inversion fraction. Therefore, for a relativly low inversion fraction of the nitrogen molecular ion N_2^+, both the air laser intensity and the number of the outer rings through the filament plasma would decrease.

It has been demonstrated that a remote pump laser at 226 nm wavelength could drive a two-photon dissociation of molecular oxygen and a two-photon excitation of one of the resulting oxygen atom fragments (Yuan *et al.* 2014). The two-photon excitation transition from the ground state to the exited state produces fluorescence emission at 845 nm, which leads to the high gain and lasing properties in the backward direction. Actually, the lasing effect could be realized by the excitation of all three main components of air with a particular pump femtosecond laser wavelength, including nitrogen, oxygen and argon. The air lasing based on the ionic nitrogen molecules has attracted particular attention due to the fruitful observed effects and the high concentration in air. Pumped by the femtosecond laser pulses at 800 nm, nitrogen ions give rise to a series of narrow emission lines at 391.4 nm, 427.8 nm and 471.2 nm. The N_2^+ lasing at 391 nm associated with the $B^2\sum_u^+ \rightarrow X^2\sum_g^+$ emission induced by the femtosecond laser filament is noteworthy among the air lasing emission lines for that the population transferring process from the ground state could be monitored. Moreover, the air lasing at 391 nm has been commonly observed in the experiments under certain conditions. Therefore, in this study, we mainly

https://doi.org/10.1017/S0022377824000783 Published online by Cambridge University Press

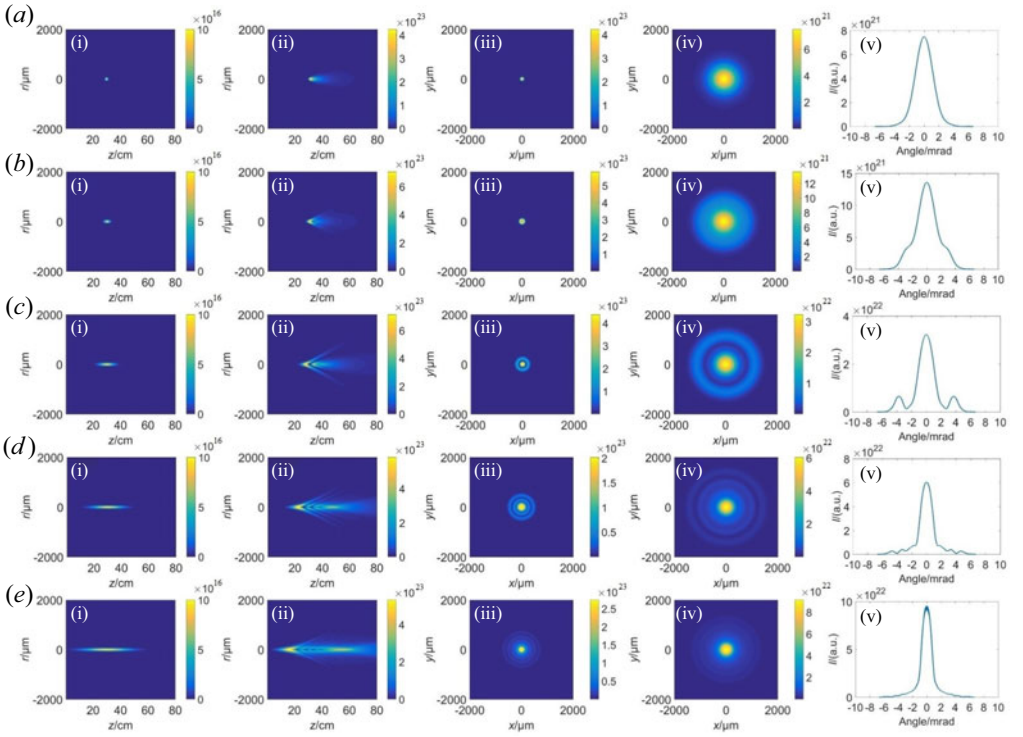

FIGURE 1. (*a*1)–(*e*1) Spatial distributions of the filament-induced nitrogen ion density versus propagation distance for different filament lengths. (*a*2)–(*e*2) Spatial distributions of the air laser intensity along the propagation direction. (*a*3)–(*e*3) Transverse patterns of air laser intensity distributions at the right end of the filament. (*a*4)–(*e*4) Transverse patterns of air laser intensity distributions at the distance of 30 cm from the right-hand end of the filament. (*a*5)–(*e*5) Divergent angular distributions of the air laser intensity. The filament lengths are (*a*) 2 cm, (*b*) 4 cm, (*c*) 10 cm, (*d*) 20 cm and (*e*) 30 cm.

focus on the air lasing at the 391.4 nm wavelength based on the ionic nitrogen molecules. The air lasing process based on the oxygen molecules was not included in the simulation.

3. Results and discussion

The air laser intensity distributions for various filament plasma lengths were investigated. The peak nitrogen ion density was chosen to be 10^{17} cm^{-3}, which could be obtained in the laser filament pumped by a tightly focused femtosecond laser. The results are indicated in figure 1. The filament lengths are 2 cm, 4 cm, 10 cm, 20 cm and 30 cm for figures 1(*a*), 1(*b*), 1(*c*), 1(*d*) and 1(*e*), respectively. Figures 1(*a*1)–1(*e*1) depict the spatial distributions of the nitrogen ion density along the propagation direction for different filament lengths. The centre of the filament plasma is at $z = 30$ cm. Figure 1(*a*2–*e*2) show the spatial distribution of the air laser beam intensity along the propagation direction. Figure 1(*a*3–*e*3) correspond to the air laser intensities on the cross-section at the right end of the filament, while figure 1(*a*4–*e*4) correspond to the beam intensity patterns on the cross-section at the distance of 30 cm from the right-hand end of the filament. Figure 1(*a*5–*e*5) refer to the divergent angular distributions of the air laser intensities.

For the filament length of 2 cm, figures 1(*a*4) and 1(*a*5) indicate that a Gaussian profile of the air laser with a divergence angle of around 2 mrad is formed. When the filament

https://doi.org/10.1017/S0022377824000783 Published online by Cambridge University Press

length reaches 4 cm, a doughnut beam pattern of the air laser occurs after propagating through the filament at $z = 32$ cm as shown in figure 1(*b*3). Figures 1(*b*4) and 1(*b*5) show that the air laser beam pattern can be regarded as the superposition of an inner Gaussian beam and an outer doughnut ring beam, resulting from the defocusing effect of the filament plasma and diffraction effect in the free space for the air laser. For the filament length of 10 cm, the inner Gaussian beam and the outer doughnut ring beam get apart from each other, as indicated in figure 1(*c*3–*c*5). As shown in figure 1(*d*), when the filament length is 20 cm, a multiple rings structure occurs on the air laser beam cross-section after passing through the filament. This could be attributed to an interesting multiple-diffraction effect for the air laser inside the filament plasma. At the beginning of the air laser propagating in the filament plasma, since the lasing effect of the stimulated fluorescence overcomes the diffraction effect induced by the filament plasma, the air laser intensity gets increased with the propagating distance. After the air laser passes through the filament for several centimetres, the gain effect and the diffraction effect get balanced, leading to the highest value of the air laser intensity. Then the air laser intensity starts to drop down as the diffraction effect overcomes the lasing effect. During this process, an outer ring structure forms on the cross-section of the air laser beam. For a relatively long filament length, this dynamic process could be repeated for several times, resulting in a multiple rings structure pattern of the air laser. This is the so-called multiple-diffraction phenomenon proposed in this paper. Further, for the filament length of 30 cm, the number of the outer rings gets larger as shown in figure 1(*e*3). At the distance $z = 75$ cm, the outer rings merge together and the outline of the air laser intensity divergent angular distribution becomes smooth as indicated in figures 1(*e*4) and 1(*e*5).

For the lasing action around 391 nm self-seeded by the second harmonic around 400 nm generated by the laser pulse in the filament plasma, the backward stimulated emission was relatively weak compared with the forward one, which was demonstrated in the experiment (Liu *et al.* 2013). The second harmonic generation was attributed to the non-uniform plasma distribution driven by the ponderomotive force or an electric-field-induced third-order mixing, leading to the difference of the harmonic intensity between the forward and backward directions. Conversely, it has been demonstrated that the air laser at 845 nm with a high gain can be achieved in the near-infrared region by pumping with a focused ultraviolet laser. Moreover, the lasing is equally strong in the forward and backward directions (Dogariu *et al.* 2011). In this study, it is assumed that the filament plasma is uniformly distributed. The lasing action is initiated by fluorescence emission whose intensity depends on the filament plasma distribution, leading to equally strong lasing in both forward and backward directions. Therefore, both backward and forward propagation of air lasing could be assumed in the simulation.

Further, the air laser intensity spatial distributions for different peak nitrogen ion densities were studied. The filament length was set to be 20 cm. The nitrogen ion densities are 10^{16} cm^{-3}, 5×10^{16} cm^{-3}, 10^{17} cm^{-3}, 1.2×10^{17} cm^{-3} and 1.4×10^{17} cm^{-3} for figures 2(*a*), 2(*b*), 2(*c*), 2(*d*) and 2(*e*), respectively. Figure 2(*a*1–*e*1) show the spatial distributions of the air laser intensity along the propagation direction, while figure 2(*b*2–*e*2) represent the air laser beam patterns on the cross-section at propagation distance of 70 cm. The corresponding divergent angular distributions of the air laser intensity are depicted in figure 2(*a*3–*e*3). Figure 2(*a*4–*e*4) depict the air laser intensity at the centre of the cross-section as a function of propagation distance.

As shown in figures 2(*a*2) and 2(*a*3), for a relative low peak nitrogen ion density of 10^{16} cm^{-3}, a super-Gaussian profile of the air laser occurs after the filament plasma with a divergent angle of around 2 mrad. Inside the filament, the air laser peak intensity increases due to the lasing effect and then decreases induced by the diffraction effect. Moreover,

https://doi.org/10.1017/S0022377824000783 Published online by Cambridge University Press

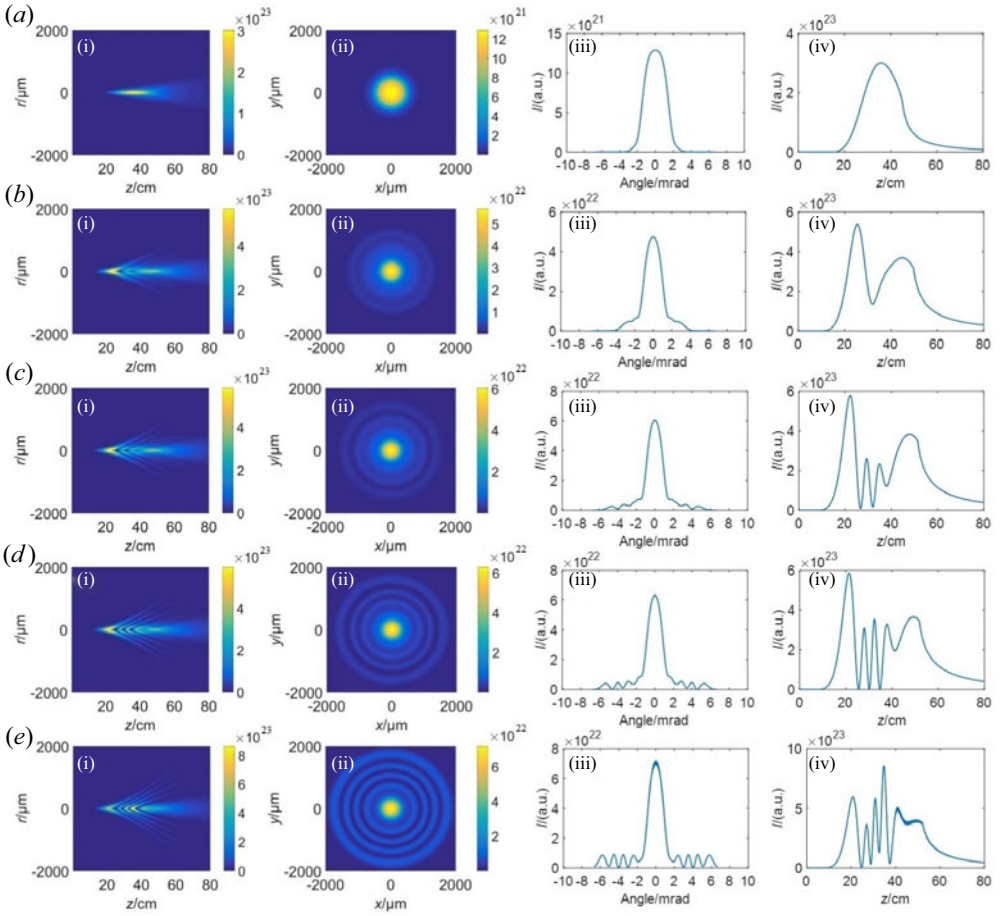

FIGURE 2. (*a*1)–(*e*1) Spatial distributions of the air laser intensity along the propagation direction for different nitrogen ion densities. (*b*2)–(*e*2) Transverse patterns of the air laser intensity at distance of 70 cm. (*b*3)–(*e*3) Divergent angular distributions of the air laser intensity. (*b*4)–(*e*4) The air laser intensity at the centre of the beam cross-section as a function of propagation distance. The peak nitrogen ion densities are (*a*) 10^{16} cm^{-3}, (*b*) 5×10^{16} cm^{-3}, (*c*) 10^{17} cm^{-3}, (*d*) 1.2×10^{17} cm^{-3} and (*e*) 1.4×10^{17} cm^{-3}.

there exists only one peak as shown in figure 2(*a*4). The outer ring structure of the air laser is formed with the peak nitrogen ion density of 5×10^{16} as indicated in figure 2(*b*). There are two peaks for the air laser intensity at the centre of the cross-section along the propagation direction as shown in figure 2(*b*4), resulting from the multiple-diffraction effect induced by a relative high nitrogen ion density distribution. By increasing the peak nitrogen ion density of the filament plasma, both the number of the outer rings for the air laser and the number of the peaks of the central air laser intensity along the propagation direction increase as shown in figure 2(*c*–*e*). It is worth mentioning that the peak intensities of the air laser along the propagation direction for different nitrogen ion density distributions almost remain at a constant order of magnitude due to the balance between the lasing effect and the diffraction effect.

In a previous experimental study (Liu *et al.* 2013), the lasing radiation profiles around 391 nm exhibits a Gaussian pattern in the nitrogen gas with a relatively low pressure.

https://doi.org/10.1017/S0022377824000783 Published online by Cambridge University Press

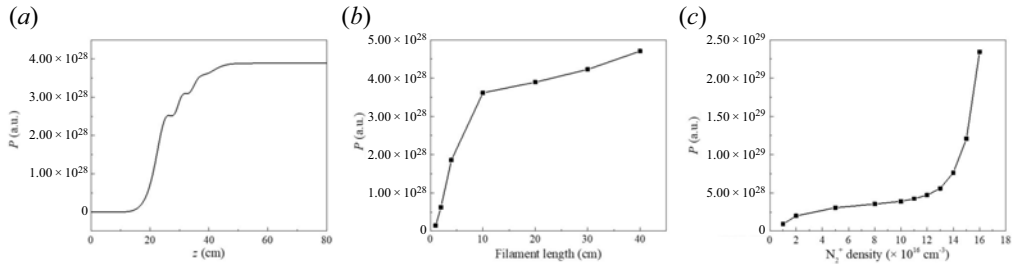

FIGURE 3. (*a*) Air laser beam power along the propagation direction for filament length of 20 cm and peak nitrogen ion density of 10^{17} cm^{-3}. (*b*) The laser beam power after the filament plasma as a function of the filament length. (*c*) The laser beam power after the filament plasma as a function of the peak nitrogen ion density.

Upon increase of nitrogen gas pressure, an outer ring structure surrounding the central spot appears. This result is consistent with the simulation result in figure 2, which shows the same variation of the lasing radiation profile with the increase of the nitrogen ion density. This experimental result can be clarified by the multiple-diffraction effect induced by the relative high nitrogen ion density. In Zeng *et al.* 2014, angular distribution of the backscattered nitrogen fluorescence induced by femtosecond laser filamentation in air has been studied in the experiment. Air lasing emission at 357 nm also forms a multiple rings profile.

A representative result for the air laser beam power along the propagation direction is shown in figure 3(*a*). The filament length is chosen to be 20 cm, while the peak nitrogen ion density is 10^{17} cm^{-3}. The result indicates that the air laser experiences a gain effect inside the filament plasma and the beam power remains constant after passing through the filament. Figure 3(*b*) represents the air laser beam power after the filament as a function of the filament length. The amplified air laser beam power increases heavily when the filament length is less than 10 cm. Since the propagation of the air laser inside the filament for one time of diffraction is almost within 10 cm, the gain effect overcomes the diffraction effect during this filament region. Thus, the air laser beam intensity experience increasing continuously inside the filament. When the filament length is larger than 10 cm, the increase slope of the amplified air laser power versus the filament length drops down. This results from the multiple-diffraction effect. Since in some parts of the filament the diffraction effect overcomes the gain effect, the air laser beam intensity cannot increase continuously.

In addition, the laser beam power after the filament plasma as a function of the peak nitrogen ion density has been investigated as shown in figure 3(*c*). The filament length is set to be 20 cm. Since the lasing effect overcomes the diffraction effect for a relatively low nitrogen ion density, the air laser power increases heavily when the peak nitrogen ion density is less than 5×10^{16} cm^{-3}. Then the air laser power increases slowly with the peak nitrogen ion density larger than 5×10^{16} cm^{-3}. When the peak nitrogen ion density is larger than 1.2×10^{17} cm^{-3}, the air laser power increases almost exponentially versus the peak nitrogen ion density. This is caused by the fact that the lasing effect of the filament plasma plays a dominant role in the propagating of the air laser for a relatively large nitrogen ion density.

When the incident pulse energy was below the energy threshold for harmonic generation, external seeding pulse was required to initiate lasing action of N_2^+. Lasing emission around 391 nm could also self-seeded by the second harmonic around 400 nm

https://doi.org/10.1017/S0022377824000783 Published online by Cambridge University Press

generated by the laser pulses in the filament plasma for the case with the incident laser energy exceeding the second harmonic generation threshold energy (Liu *et al.* 2013). Self-induced white light inside the filament covering the $B^2\sum_u^+ \rightarrow X^2\sum_g^+$ transition was serving as the seed to be amplified, leading to the self-seeded lasing action at 428 nm in air. The white light seed pulse was generated through spectral broadening mechanisms such as self-phase modulation and self-steepening of the femtosecond laser pulse (Chu *et al.* 2013). In this study, the air lasing was self-seeded by the spontaneous fluorescence emission with the field amplitude depending on the nitrogen ion density in the filament plasma, which has been included in the simulation. For external seed laser passing through the filament plasma, the air laser would also form a multiple rings structure. Moreover, the multiple rings size would rely on the nitrogen ion density distribution.

4. Conclusion

In a summary, the lasing action of the fluorescence emitted from the transmission of the first negative (0,0) band of nitrogen ions at 391 nm was simulated during the femtosecond laser filamentation. The air laser intensity spatial distributions show that the beam profile changes from a Gaussian or super-Gaussian shape to an outer rings structure by increasing the filament length or nitrogen ion density. This result meets well the experimental result in a previous study. The multiple-diffraction effect induced by the dynamical interaction between the lasing effect and diffraction effect of the filament plasma causes the outer rings structure pattern of the air laser. This study provides a feasible way to understand the mechanism of the air laser propagating properties and improve the energy conversion efficiency and directivity of remote air lasers, which would be significant for remote sensing applications based on femtosecond laser filamentation.

Acknowledgements

Editor V. Malka thanks the referees for their advice in evaluating this paper.

Funding

This work was supported by the National Natural Science Foundation of China (grant number 12004316).

Declaration of interests

The authors report no conflict of interest.

Data availability

Data underlying the results presented in this paper are not publicly available at this time but may be obtained from the authors upon reasonable request.

REFERENCES

AKOZBEK, N., SCALORA, M., BOWDEN, C.M. & CHIN, S.L. 2001 White-light continuum generation and filamentation during the propagation of ultra-short laser pulses in air. *Opt. Commun.* **191**, 353–362.

BAHATI, E.M., JURETA, J.J., BELIC, D.D., CHERKANI-HASSANI, H., ABDELLAHI, M.O. & DEFRANCE, P. 2001 Electron impact dissociation and ionization of N_2^+. *J. Phys.* B **34**, 2963–2973.

BERGE, L., SKUPIN, S., NUTER, R., KASPARIAN, J. & WOLF, J.-P. 2007 Ultrashort filaments of light in weakly ionized, optically transparent media. *Rep. Prog. Phys.* **70**, 1633.

BRIAN, J. & MITCHELL, A. 1990 The dissociative recombination of molecular ions. *Phys. Rep.* **186**, 215–248.

https://doi.org/10.1017/S0022377824000783 Published online by Cambridge University Press

Chauveau, S., Perrin, M.Y., Riviere, P. & Soufiani, A. 2002 Contributions of diatomic molecular electronic systems to heated air radiation. *J. Quant. Spectrosc. Radiat. Transfer* **72**, 503–530.

Chin, S.L., Hosseini, S.A., Liu, W., Luo, Q., Theberge, F., Akozbek, N., Becker, A., Kandidov, V.P., Kosareva, O.G. & Schroeder, H. 2005 The propagation of powerful femtosecond laser pulses in opticalmedia: physics, applications, and new challenges. *Can. J. Phys*. **83**, 863.

Chiron, A., Lamouroux, B., Lange, R., Ripoche, J.F., Franco, M., Prade, B., Bonnaud, G., Riazuelo, G. & Mysyrowicz, A. 1999 Numerical simulations of the nonlinear propagation of femtosecond optical pulses in gases. *Eur. Phys. J.* D **6**, 383.

Chu, W., Li, G., Xie, H., Ni, J., Yao, J., Zeng, B., Zhang, H., Jing, C., Xu, H., Cheng, Y. & Xu, Z. 2013 A self-induced white light seeding laser in a femtosecond laser filament. *Laser Phys. Lett*. **11** (1), 015301.

Couairon, A. & Mysyrowicz, A. 2007 Femtosecond filamentation in transparent media. *Phys. Rep*. **441**, 47.

Doering, J.P. & Yang, J. 1996 Comparison of the electron impact cross section for the N_2^+ first negative (0,0) band (λ 3914 Å) measured by optical fluorescence, coincidence electron impact, and photoionization experiments. *J. Geophys. Res*. **101**, 19723.

Dogariu, A., Michael, J.B., Scully, M.O. & Miles, R.B. 2011 High-gain backward lasing in air. *Science* **331**, 442.

Dubietis, A., Tamosauskas, G., Fibich, G. & Ilan, B. 2004 Multiple filamentation induced by input-beam ellipticity. *Opt. Lett*. **29**, 1126–1128.

Jain, A., Gupta, D.N. & Suk, H. 2019 Electron–ion recombination effect on electron acceleration by an intense laser pulse. *IEEE Trans. Plasma. Sci*. **47**, 4891–4897.

Johnson, A.W. & Fowler, R.G. 1970 Measured lifetimes of rotational and vibrational levels of electronic states of N_2. *J. Chem. Phys*. **53**, 65–72.

Kandidov, V.P., Shlenov, S.A. & Kosareva, O.G. 2009 Filamentation of high-power femtosecond laser radiation. *Quant. Electron*. **39**, 205.

Kartashov, D., Alisauskas, S., Andriukaitis, G., Pugžlys, A., Shneider, M.N., Zheltikov, A.M., Chin, S.L. & Baltuska, A. 2012 Free-space nitrogen gas laser driven by a femtosecond filament. *Phys. Rev.* A **86**, 033831.

Kartashov, D. & Shneider, M.N. 2017 Femtosecond filament initiated, microwave heated cavity-free nitrogen laser in air. *J. Appl. Phys*. **121**, 113303.

Kasparian, J. & Wolf, J.-P. 2008 Physics and applications of atmospheric nonlinear optics and filamentation. *Opt. Express* **16**, 466.

Liu, W. 2014 Intensity clamping during femtosecond laser filamentation. *Chin. J. Phys*. **52**, 465.

Liu, Y., Brelet, Y., Point, G., Houard, A. & Mysyrowicz, A. 2013 Self-seeded lasing in ionized air pumped by 800 nm femtosecond laser pulses. *Opt. Express* **21**, 22791.

Liu, W. & Chin, S.L. 2007 Abnormal wavelength dependence of the self-cleaning phenomenon during femtosecond-laser-pulse filamentation. *Phys. Rev.* A **76**, 013826.

Luo, Q., Liu, W. & Chin, S.L. 2003 Lasing action in air induced by ultrafast laser filamentation. *Appl. Phys.* B **76**, 337.

Mehr, F.J. & Biondi, M.A. 1969 Electron temperature dependence of recombination of O_2^+ and N_2^+ ions with electrons. *Phys. Rev*. **181**, 264–271.

Ni, J., Chu, W., Jing, C., Zhang, H., Zeng, B., Yao, J., Li, G., Xie, H., Zhang, C., Xu, H., Chin, S.-L., Cheng, Y. & Xu, Z. 2013 Identification of the physical mechanism of generation of coherent N_2^+ emissions in air by femtosecond laser excitation. *Opt. Express* **21**, 8746.

Sprangle, P., Penano, J., Hafizi, B., Gordon, D. & Scully, M. 2011 Remotely induced atmospheric lasing. *Appl. Phys. Lett*. **98**, 211102.

Wang, Q., Ding, P., Wilkins, S.G., Athanasakis-Kaklamanakis, M., Zhang, Y., Liu, Z. & Hu, B. 2023 Theoretical treatment on externally-seeded superradiance from N_2^+ in femtosecond laser filamentation in low-pressure nitrogen. *Front. Phys*. **10**, 1090346.

Xu, H.L., Azarm, A., Bernhardt, J., Kamali, Y. & Chin, S.L. 2009 The mechanism of nitrogen fluorescence inside a femtosecond laser filament in air. *Chem. Phys*. **360** (1–3), 171–175.

XUE, J., ZHANG, N., GUO, L., ZHANG, Z., QI, P., SUN, L., GONG, C., LIN, L. & LIU, W. 2022 Effect of laser repetition rate on the fluorescence characteristic of a long-distance femtosecond laser filament. *Opt. Lett*. **47**, 5676–5679.

YAO, J., CHU, W., LIU, Z., CHEN, J., XU, B. & CHENG, Y. 2018 An anatomy of strong-field ionization-induced air lasing. *Appl. Phys.* B **124**, 1–17.

YAO, J., ZENG, B., XU, H., LI, G., CHU, W., NI, J., ZHANG, H., CHIN, S.L., CHENG, Y. & XU, Z. 2011 High-brightness switchable multiwavelength remote laser in air. *Phys. Rev.* A **84** (5), 051802.

YUAN, S., WANG, T., LU, P., CHIN, S.L. & ZENG, H. 2014 Humidity measurement in air using filament-induced nitrogen monohydride fluorescence spectroscopy. *Appl. Phys. Lett*. **104**, 091113.

YUAN, S., WANG, T., TERANISHI, Y., SRIDHARAN, A., LIN, S.H., ZENG, H. & CHIN, S.L. 2013 Lasing action in water vapor induced by ultrashort laser filamentation. *Appl. Phys. Lett*. **102**, 224102.

ZENG, T., ZHAO, J.Y., LIU, W. & CHIN, S.L. 2014 Backward angular distribution of air lasing induced by femtosecond laser filamentation. *Laser Phys. Lett*. **11** (7), 075401.

ZHANG, X., LU, Q., ZHANG, Z., FAN, Z., ZHOU, D., LIANG, Q., YUAN, L., ZHUANG, S., DORFMAN, K. & LIU, Y. 2021 Coherent control of the multiple wavelength lasing of N_2^+: coherence transfer and beyond. *Optica* **8** (5), 668–673.

ZHOU, D., ZHANG, X., LU, Q., LIANG, Q. & LIU, Y. 2020 Time-resolved study of the lasing emission from high vibrational levels of N_2^+. *Chin. Opt. Lett*. **18**, 023201.

https://doi.org/10.1017/S0022377824000783 Published online by Cambridge University Press